Journal of Pathology
J Pathol 2012; **227:** 417–430
Published online in Wiley Online Library
(wileyonlinelibrary.com) DOI: 10.1002/path.4053

ORIGINAL PAPER

Anti-VEGF antibody therapy does not promote metastasis in genetically engineered mouse tumour models

Mallika Singh,[#†] Suzana S Couto,[†] William F Forrest, Anthony Lima, Jason H Cheng, Rafael Molina, Jason E Long, Patricia Hamilton, Angela McNutt, Ian Kasman, Michelle A Nannini, Hani Bou Reslan, Tim C Cao, Calvin CK Ho, Kai H Barck, Richard AD Carano, Oded Foreman, Jeffrey Eastham-Anderson, Adrian M Jubb, Napoleone Ferrara and Leisa Johnson[†*]

Genentech Inc., 1 DNA Way, South San Francisco, CA, USA

**Correspondence to: Leisa Johnson or Mallika Singh, Genentech Inc., 1 DNA Way, Room 12-322 (MS 37), South San Francisco, CA 94080, USA. e-mail: johnson.leisa@gene.com or msingh@gene.com*

[†]These authors contributed equally.
[#]Current address: Novartis Institutes for Biomedical Research, 4560 Horton Street, Emeryville, CA 94608, USA.

Abstract

Resistance to anti-angiogenic therapy can occur via several potential mechanisms. Unexpectedly, recent studies showed that short-term inhibition of either VEGF or VEGFR enhanced tumour invasiveness and metastatic spread in preclinical models. In an effort to evaluate the translational relevance of these findings, we examined the consequences of long-term anti-VEGF monoclonal antibody therapy in several well-validated genetically engineered mouse tumour models of either neuroendocrine or epithelial origin. Anti-VEGF therapy decreased tumour burden and increased overall survival, either as a single agent or in combination with chemotherapy, in all four models examined. Importantly, neither short- nor long-term exposure to anti-VEGF therapy altered the incidence of metastasis in any of these autochthonous models, consistent with retrospective analyses of clinical trials. In contrast, we observed that sunitinib treatment recapitulated previously reported effects on tumour invasiveness and metastasis in a pancreatic neuroendocrine tumour (PNET) model. Consistent with these results, sunitinib treatment resulted in an up-regulation of the hypoxia marker GLUT1 in PNETs, whereas anti-VEGF did not. These results indicate that anti-VEGF mediates anti-tumour effects and therapeutic benefits without a paradoxical increase in metastasis. Moreover, these data underscore the concept that drugs targeting VEGF ligands and receptors may affect tumour metastasis in a context-dependent manner and are mechanistically distinct from one another.

Keywords: VEGF; sunitinib; metastasis; efficacy; cancer; mouse; preclinical; genetically; engineered; models

Received 16 April 2012; Revised 5 May 2012; Accepted 10 May 2012

Conflict of interest: all authors are/were employees of Genentech, a member of the Roche Group, and have/had financial holdings in Genentech/Roche during the course of this work. Genentech/Roche owns all patent rights.

Introduction

Anti-angiogenic agents represent a class of drugs that target the tumour vasculature and can be successfully combined with other anti-cancer therapies [2,3]. Targeting vascular endothelial growth factor A (VEGF) or its tyrosine kinase receptors (VEGFR-1 and VEGFR-2) is the strategic basis of all anti-angiogenic drugs currently approved to treat cancer and intraocular neovascular disorders, with several additional clinical trials with similar agents under way [4,5]. The anti-VEGF monoclonal antibody bevacizumab (Avastin®) was the first anti-angiogenic cancer drug approved by the US FDA [6], followed by the approval of five small-molecule receptor tyrosine kinase inhibitors (RTKIs; sunitinib, sorafenib, pazopanib, vandetanib and axitinib) that inhibit signalling through VEGFRs and a variety of other RTKs [7]. All of these anti-angiogenic agents have shown therapeutic success in a wide variety of tumour types, albeit often in combination with chemotherapy. However, not all cancer patients benefit from such therapies and some who show benefit initially can develop resistance to these drugs [8]. Over the last few years, several mechanisms of inherent refractoriness or acquired resistance to anti-angiogenic therapies have been described, including factors elaborated by tumour-infiltrating myeloid cells or fibroblasts [9–13].

Recent preclinical findings have raised an interesting conundrum observed in some instances of anti-angiogenic therapy: three studies in multiple mouse models found that while targeted inhibition of VEGF signalling effectively treated the primary cancer, it

also resulted in a more invasive tumour morphology and increased frequencies of metastatic lesions [14–16]. These phenomena appeared irreversible, in that discontinuation of treatment did not alter the observed occurrences of metastasis [15]. The initial studies were carried out using two VEGFR-2 inhibitors as single agents, namely the small-molecule RTKI sunitinib/SU11 248 (Sutent®) and the monoclonal antibody DC101 [14,15]; a more recent set of experiments employed a polyclonal goat anti-VEGF antibody [16]. Altogether, these reports broadly implied that clinical application of all anti-angiogenic therapies could potentiate an increase in metastasis despite attenuation of primary tumour growth [8,17]. Consequently, such an increased frequency of metastasis could compromise therapeutically derived progression-free survival (PFS) and/or overall survival (OS) benefits, and ultimately contribute to resistance to anti-angiogenic treatment. However, none of these preclinical studies examined metastatic incidence following long-term anti-angiogenic treatment. Rather, the examinations of metastatic incidence were limited to short-term treatment settings, which are difficult to extrapolate and compare with clinical endpoints such as PFS and OS.

We set out to ask whether short- or long-term bevacizumab therapy altered the incidence of tumour invasion and metastasis in multiple genetically engineered mouse tumour models (GEMMs). To address this question, we used a well-characterized monoclonal anti-VEGF antibody, named B20-4.1.1 (hereinafter referred to as 'anti-VEGF'), which binds murine VEGF with an affinity similar to that of bevacizumab for human VEGF and is suitable for long-term studies in immune-competent mice [1]. We examined four different GEMMs with varied metastatic potential and responses to anti-VEGF. Where relevant to the clinical setting, we also assessed anti-VEGF in combination with chemotherapy. GEMMs are an advantageous platform to interrogate agents that target the tumour microenvironment, as all the cellular components of the spontaneous cancers co-evolve within the appropriate organ throughout neoplastic progression, closely mimicking the multi-step process of human carcinogenesis [18–20]. We have previously shown that two mutant *Kras*-driven models of human pancreatic ductal adenocarcinoma (PDAC) and non-small cell lung cancer (NSCLC, adenocarcinoma subtype) can serve as good models for assessing therapeutic response to standard-of-care chemotherapies in combination with targeted agents, including anti-VEGF [1]. Here, in addition to these two epithelial cancer models, we also investigated the consequences of anti-VEGF therapy upon tumour invasion and metastasis in two neuroendocrine tumour models driven by simultaneous *Rb* and *p53* inactivation: a SV40 large T-antigen-driven transgenic pancreatic neuroendocrine tumour (PNET) model that phenocopies the prototype *Rip-Tag* model [21], and a previously described conditional model for small cell lung carcinoma (SCLC) [22].

Materials and methods

Animal experiments

We obtained mice from the following institutions: $Kras^{LSL-G12D}$ from Tyler Jacks (Massachusetts Institute of Technology); $p53^{frt/frt}$ and *RIP-TβAg* from Exelixis Inc.; $p16/p19^{fl/fl}$ and $Rb^{fl/fl}$ from Anton Berns (NKI, The Netherlands); and *Pdx1-Cre* from Andy Lowy (University of Ohio). For the lung cancer models, $Kras^{LSL-G12D}$; $p53^{frt/frt}$ and $Rb^{fl/fl}$; $p53^{frt/frt}$ mice were infected at 7–9 weeks of age with 5e6 or 1e7 infectious units, respectively, of recombinant, replication-deficient adenovirus serotype 5 expressing the FLPe and Cre recombinases, as described [1]. The animals were dosed and monitored according to guidelines from the Institutional Animal Care and Use Committee (IACUC) at Genentech Inc. All chosen dosing regimens (see Supplementary materials and methods) were well tolerated in the GEMMs.

Results

Anti-VEGF monotherapy in the *RIP-TβAg* PNET model is efficacious and, unlike sunitinib, does not increase metastasis

To understand the effects of anti-VEGF in a GEMM comparable to the widely used *Rip-Tag* model, we evaluated and compared the consequences of B20-4.1.1 monoclonal antibody treatment to sunitinib therapy in a similar model of pancreatic insulinoma model named *RIP-TβAg* (Supplementary Figure S1A–H). As previously reported, long-term anti-VEGF treatment resulted in a significant OS benefit in this model [23] (Figure 1A). To compare our experiments with previous reports [15], we evaluated efficacy after 21 days of anti-VEGF or sunitinib treatment in 11–12 week-old, late-stage tumour-bearing mice, ie a regression trial [24]. As expected, both anti-VEGF and sunitinib treatment resulted in marked decreases in pancreatic tumour burden and tumour vascular density relative to controls (Figure 1B, C, Supplementary Figure 1I) [14,16]. Intriguingly, we observed differential treatment effects on the number of solid PNET tumours; relative to controls, anti-VEGF treatment reduced the number of grossly detectable tumours per pancreas, whereas sunitinib treatment increased their number (Supplementary Figure 1J). Moreover, sunitinib treatment uniquely resulted in increased tumour hypoxia, as assessed via the immunohistochemical marker glucose transporter 1 (GLUT1) (Figure 1D, Supplementary Figure 1K). Interestingly, we did not observe differences in another hypoxia marker, carbonic anhydrase 9 (CA9), neither did we see up-regulation of cMET expression, as reported by Sennino *et al* (Supplementary Figure 1K) following treatment with either drug.

We next evaluated the effects of anti-VEGF and sunitinib on tumour invasion, using a histological

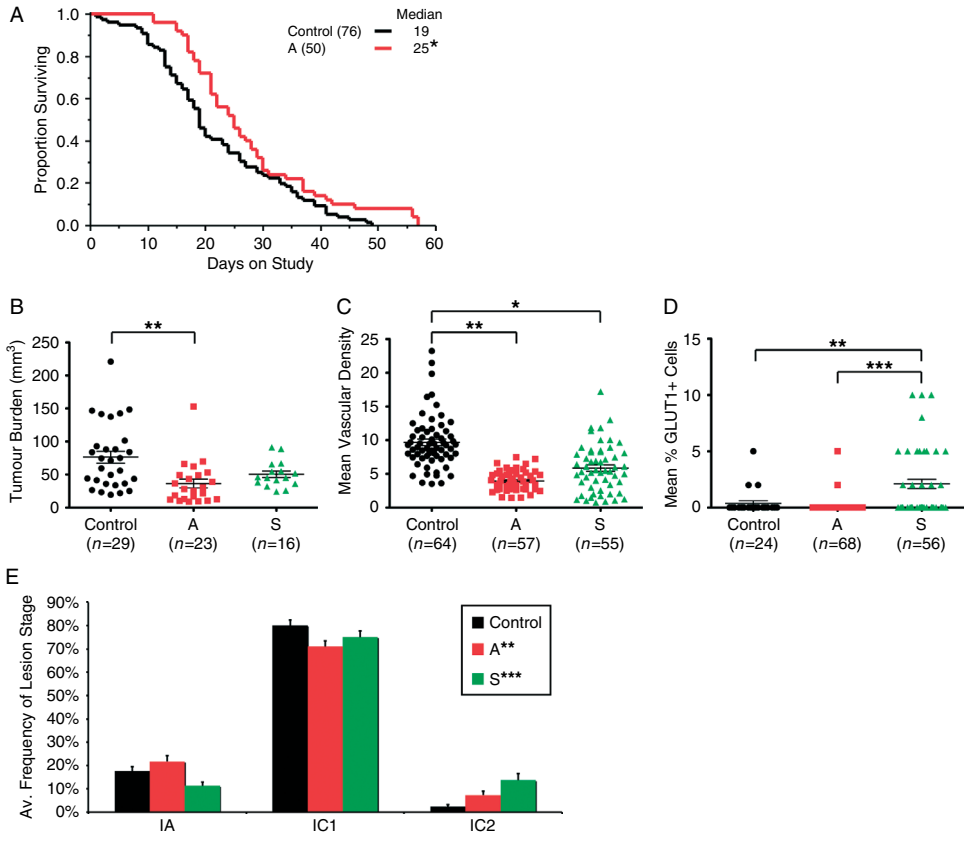

G

Treatment	Rip-TbAg, short-term (21d): # of Positive Mice / Total # Examined					
	Regional Lymph Node Metastases		Liver Metastases		Metastases to Additional Sites* (Macro &/or Micro)	Total # Mice with any Confirmed Mets (Macro &/or Micro)
	Macro	Micro	Macro	Micro		
Control	0/29	1/27	0/29	0/29	0/29	1/29
Anti-VEGF	0/23	1/20	0/23	0/22	0/23	1/23
Sunitinib	0/16	3/15	0/16	2/15*	0/16	5/16**

*Spleen, Kidney, Adrenal Glands, Reproductive Tract

Figure 1. Anti-VEGF versus sunitinib monotherapy treatment effects in the *RIP-TβAg* model of pancreatic insulinoma. Kaplan–Meier plots showing overall survival (OS) in control (black) and anti-VEGF (A, red)-treated mice; $^{*}p < 0.05$, log-rank (A). Tumour volume in control (black), anti-VEGF (A, red) and sunitinib (S, green)-treated mice at 21 days of treatment. Each dot represents the total tumour burden in an individual mouse, with the mean values ± standard error of the mean (SEM) depicted. The number of mice examined is indicated below each set. Statistical significance was assessed using pairwise contrasts based on the Tukey HSD (studentized range) method; $^{**}p < 0.005$ (B). Microvascular density in a subset of tumours and mice from (B). The number of individual tumours analysed is indicated below each set and came from five independent control-, anti-VEGF- or sunitinib-treated mice. Each dot represents vascular area/tumour area, with mean values ± SEM depicted. Statistical significance was assessed using pairwise contrasts based on the Tukey HSD (studentized range) method; $^{*}p < 0.05$, $^{**}p < 0.005$ (C). Quantitative analysis of GLUT1 expression in a subset of tumours and mice from (B). The total number of tumours analysed is indicated below each cohort and came from three independent mice/cohort. Each dot represents the percentage of cells within a given lesion that were positive for membranous GLUT1 expression; mean values ± SEM are depicted. Statistical significance was assessed using a one-tailed unpaired Student's *t*-test; $^{**}p < 0.005$, $^{***}p < 0.0005$ (D). Quantification of PNET stage and grade (IA, IC1, and IC2) frequency as a function of short-term (21 days) treatment with control (black bars), anti-VEGF (A, red bars) or sunitinib (S, green bars). The frequency of each lesion stage and grade was first calculated for individual mice and then averaged across their respective treatment cohort; mean values ± SEM are depicted. The numbers of mice, total number of lesions as well as each lesion stage and grade, and average numbers of lesions per mouse analysed per treatment cohort are summarized in Supplementary Figure 1M. Statistical significance was assessed using a cumulative link mixed model fitted with the Laplace approximation; $^{**}p < 0.005$, $^{***}p < 0.0005$ (E). Representative H&E- and insulin IHC-stained photomicrographs of metastatic PNET in the regional lymph node (RLN) and liver (LV) (F). Frequency of RLN and LV metastases observed upon gross necropsy (macro) and histological analysis (micro) in mice from (B–F). The frequency of LV metastases, as well as all metastases in the sunitinib-treated cohort, is significantly different from the other two cohorts according to a χ^2 test; $^{*}p < 0.05$, $^{**}p < 0.005$ (G). Mice were dosed with anti-ragweed control or anti-VEGF/B20-4.1.1 antibody intraperitoneally (i.p.), 5 mg/kg, once a week; sunitinib was dosed orally (p.o.), 40 mg/kg qd (daily). PNET, pancreatic neuro-endocrine tumour; IA, islet adenoma; IC1, micro-invasive carcinoma; IC2, macro-invasive carcinoma.

grading scheme for PNETs as previously described [25] (Figure 1E, Supplementary Figure 1L, M). We observed a small but statistically significant increase only in the occurrence of infrequent macro-invasive carcinomas (IC2s) in the anti-VEGF-treated cohort. In contrast, sunitinib treatment resulted in a clear and statistically significant shift in the distribution of both solid tumour stage and grade, ie decreased numbers of relatively benign adenomas (IAs) and micro-invasive carcinomas (IC1s), with a corresponding increase in IC2s. Concordant with these data, we observed no differences in the incidence of lymph node (LN) and liver (LV) metastases in the anti-VEGF treatment group relative to controls, whereas sunitinib treatment caused increased numbers of both LN and LV metastases (Figure 1F, G).

Anti-VEGF monotherapy or combination treatment with chemotherapy does not increase tumour invasiveness or metastatic potential in a SCLC GEMM

Next, we assessed the effects of anti-VEGF treatment in a second neuroendocrine tumour type, small cell lung cancer, also driven by *Rb* and *p53* tumour suppressor inactivation [26]. In contrast to PNET, human SCLC and the corresponding $Rb^{fl/fl}$; $p53^{frt/frt}$ GEMM tumours exhibit extensive and multiple regional and distant metastases [22,27]. We first carried out an in-depth characterization of disease progression in this $Rb^{fl/fl}$; $p53^{frt/frt}$ model (Supplementary Figure 2A–G). Based on this assessment, preclinical trials were initiated on mice with advanced/extensive-stage disease at 32–35 weeks postinfection (wpi). Long-term anti-VEGF monotherapy is minimally efficacious in this GEMM and did not significantly impact primary tumour burden at 4 weeks (Figure 2A, Supplementary Figure 2H), although a non-significant trend towards an OS benefit relative to control was observed (Figure 2B). Since patients with SCLC are treated with aggressive chemotherapy, and clinical trials testing combinations with bevacizumab are under way [28–30], we also assessed the long-term response of this model to a standard combination of carboplatin and irinotecan/CPT-11, with and without anti-VEGF. Chemotherapy treatment resulted in significant tumour growth inhibition and, while the addition of anti-VEGF did not significantly further enhance tumour shrinkage, we observed a remarkable combinatorial effect on OS (Figure 2A, B, Supplementary Figure 2H). We then examined long-term treatment effects on tumour invasiveness by histologically scoring neoplastic lesion stage and grade [22], and found a decrease in the average frequency of advanced/late-stage carcinomas (LS-SCLC) in both anti-VEGF-containing regimens (Supplementary Figure 2I–J; 10–20 week interval). Next, we evaluated the incidence of metastases; the likelihood of metastasis to an organ was estimated using gross observations from mice necropsied when moribund or immediately post-mortem. Grossly observed metastases were confirmed histologically when possible [regional/mediastinal lymph nodes (RLNs) were often not retained in archived samples], and there was a complete correlation between both types of observations in this model. Anti-VEGF treatment alone or in combination with chemotherapy resulted in a trend towards decreased metastatic frequency to any organ (Supplementary Figure 2K, L). These data (Supplementary Figure 2M) were then used to estimate time-indexed, regimen-specific probabilities that an organ would remain metastasis-free and summarized as a 'time to metastasis scale factor' for the two primary sites, the RLNs (Figure 2C) and LV (Figure 2D). We found no significant differences in the relative probability of observing metastasis to either organ in all treatment cohorts as compared to control, with one exception — the likelihood of both sites remaining free of metastases was significantly increased in the combination group. Finally, we examined the consequences of short-term, 14 day treatment with single-agent anti-VEGF therapy on the number, appearance and frequency of neoplastic lesion stage and grade as well as metastases (Figure 2E–G, Supplementary Figure 2N) and found no significant differences between the control and anti-VEGF-treated cohorts for any of these metrics.

Metastasis in a mutant *Kras*-driven PDAC GEMM is unaffected by anti-VEGF mono- or combination therapy

We next evaluated anti-VEGF effects in the $Kras^{LSL-G12D}$; $p16/p19^{fl/fl}$; *Pdx1-Cre* mouse model of PDAC [31]. As described previously, we performed late-stage preclinical trials in these mice and used non-invasive ultrasound imaging to follow tumour growth [1]. This model is refractory to anti-VEGF monotherapy but shows a bi-modal response to the combination with standard-of-care gemcitabine chemotherapy, as measured by primary tumour burden and OS [1] (Figure 3A, B, Supplementary Figure 3A). We did not carry out a quantitative analysis of tumour invasion, as the invasive ductal adenocarcinomas in this model present with mixed differentiation levels, thereby precluding a systematic grading assessment (Supplementary Figure 3B). Importantly, we did not observe any alterations in this mixed tumour morphology within any of the treatment cohorts, as evaluated by both haematoxylin and eosin (H&E) staining and the pancreatic ductal epithelial marker cytokeratin 19 (Supplementary Figure 3C). Similar to human PDAC, the mouse model manifests extensive regional and distant metastases, some of which were grossly apparent but many were only detectable microscopically [31]. Following a comprehensive histological analysis of short- and long-term treatment effects on the two most frequent sites of metastasis, the RLNs and the LV, we found that neither of the single or combination regimens demonstrated any significant changes in the probability or frequency of metastases to these two sites

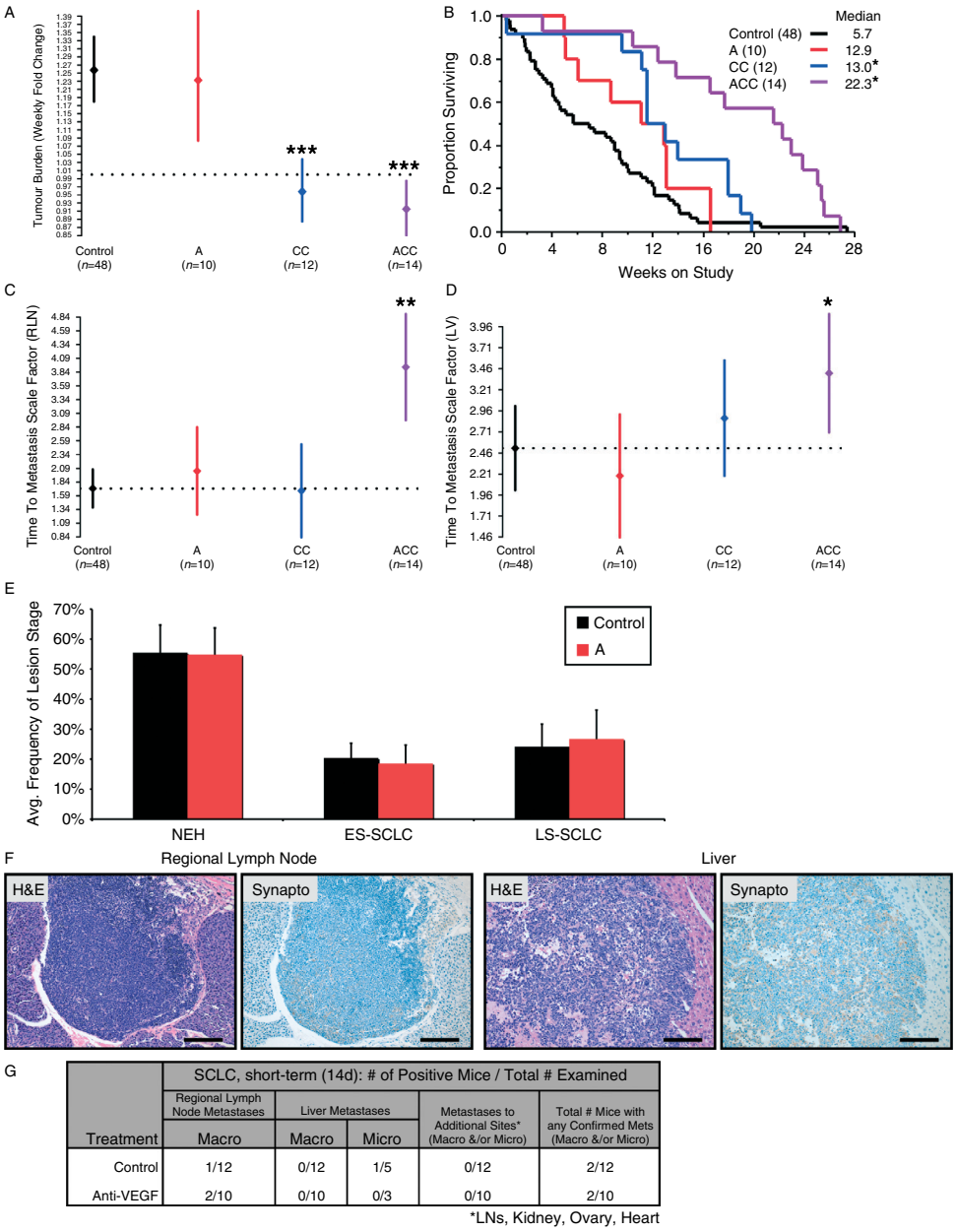

G

Treatment	SCLC, short-term (14d): # of Positive Mice / Total # Examined				
	Regional Lymph Node Metastases	Liver Metastases		Metastases to Additional Sites* (Macro &/or Micro)	Total # Mice with any Confirmed Mets (Macro &/or Micro)
	Macro	Macro	Micro		
Control	1/12	0/12	1/5	0/12	2/12
Anti-VEGF	2/10	0/10	0/3	0/10	2/10

*LNs, Kidney, Ovary, Heart

Figure 2. Anti-VEGF treatment effects on primary tumour burden, overall survival and metastasis in a genetically engineered mouse model of SCLC, regression setting. Weekly fold-change in tumour burden, as measured by micro-CT for each treatment cohort: control (black), anti-VEGF (A, red), carboplatin plus CPT-11 (irinotecan) chemotherapy (CC, blue) and the combination of anti-VEGF plus chemotherapy (ACC, purple). Data are shown as mean ±95% confidence intervals; $^{***}p < 0.0005$ (A). Kaplan–Meier plots showing OS in treatment cohorts described in (A); $^{*}p < 0.05$, log-rank (B). Weibull scale factors estimated by modelling the probability of remaining free of metastases to the RLN (C) or LV (D) for the long-term treatment cohorts shown in (A and B). The number of mice examined per treatment cohort is indicated below each point. Data are shown as mean ±95% confidence intervals; $^{*}p < 0.05$, $^{**}p < 0.005$. Quantification of SCLC lesion stage and grade (NEH, ES-SCLC and LS-SCLC) frequency as a function of short-term (14 days) treatment with either control (black bars) or anti-VEGF (A, red bars). The frequency of each lesion stage and grade was first calculated for individual mice and then averaged across their respective treatment cohorts; mean values ± SEM are depicted. The numbers of mice, total number of lesions as well as each lesion stage and grade, and average numbers of lesions per mouse analysed per treatment cohort are summarized in Supplementary Figure 2N. Statistical significance was assessed using a cumulative link mixed model fitted with the Laplace approximation. None of the observations were significantly different from one another (E). Representative H&E and synaptophysin IHC-stained photomicrographs of metastatic SCLC in the RLN and LV (F). Frequency of RLN and LV metastases observed upon gross necropsy (macro) and histological analysis (micro, LV only) in mice from the short-term treatment experiment from (E, F). All macro- and micro-metastasis observations in this model show complete correlation, and no significant differences were found between any treatment groups for metastatic frequency to a given tissue or total metastatic incidence to any organ (G). Mice were dosed with anti-ragweed control or anti-VEGF/B20-4.1.1 antibody i.p., 5 mg/kg, twice weekly; CPT-11/irinotecan was dosed i.p., 80 mg/kg, q4d × 6; carboplatin was dosed i.p. at either 30 mg/kg, q4d × 6 (long-term study) or 25 mg/kg, qd × 5 (14 day short-term study). SCLC, small cell lung cancer; Micro-CT, micro-computed tomography; NEH, neuroendrocrine hyperplasia; ES-SCLC, early-stage SCLC; LS-SCLC, late-stage SCLC; LNs, lymph nodes.

(and others) relative to controls (Figure 3C–F, Supplementary Figure 3D, E). While we observed a small, albeit insignificant, trend towards a decreased time to metastasis scale factor with anti-VEGF monotherapy relative to controls, these data are difficult to interpret in the absence of a clear OS difference between the two groups. However, the defined, short-term, 7 day time point analysis clearly showed that neither anti-VEGF or gemcitabine, nor the combination, significantly altered metastasis to RLNs or the LV as compared to controls (Figure 3F).

Anti-VEGF mono- or combination therapy does not increase tumour invasiveness or metastatic potential in a NSCLC GEMM

Next, we tested the $Kras^{LSL-G12D}$; $p53^{frt/frt}$ mouse model of NSCLC, where treatment with anti-VEGF mono- and combination therapy with carboplatin significantly affected tumour growth inhibition and OS benefit relative to controls [1] (Figure 4A, B, Supplementary Figure 4A). Here, we also compared the effects of anti-VEGF treatment discontinuation after 14 days with continuous therapy; 14 days is sufficient time to observe an effect on tumour burden by micro-CT imaging. We found that the 14 day treatment still demonstrated significant tumour growth inhibition after 6 weeks and resulted in a survival benefit similar to carboplatin treatment. We then assessed long-term treatment effects on tumour invasiveness by scoring the average frequency of neoplastic lesion stage and grade [32,33] (Supplementary Figure 4B, C). Anti-VEGF-containing regimens exhibited increased average frequencies of earlier stage lesions (AAH and adenomas), with a concomitant reduction in more advanced lesions (low-grade and/or high-grade adenocarcinomas). When we evaluated metastases, we observed no increase in frequencies of mice with metastases to any organ (Supplementary Figure 4D, E) or any significant differences between treatment groups versus control in the probability analyses for RLN and LV metastases (Figure 4C, D, Supplementary Figure 4F). We were unable to calculate a time to metastasis scale factor for RLNs in the carboplatin treatment group because we did not observe any metastases in the limited number of mice available (data not shown) and for LV metastases in the anti-VEGF discontinuous cohort due to tissue availability. Similar to the long-term treatment results, short-term (14 day) therapy with anti-VEGF-containing regimens significantly reduced tumour growth rates, demonstrated the same shift towards earlier stage lesions (albeit the trend did not reach statistical significance) and did not change the frequency of metastases (Figure 4E–G, Supplementary Figure 4G, H).

Since sunitinib has/is currently being examined in various NSCLC clinical trials, we independently compared anti-VEGF and sunitinib short-term treatments in this GEMM. In contrast to anti-VEGF monotherapy, sunitinib treatment (using the same dose and drug stock as in the PNET model) did not significantly impact tumour growth, lesion stage and grade distribution, the occurrence of metastases or the micro-vascular density in any neoplastic stage (Supplementary Figure 4I–O). We also examined anti-VEGF and sunitinib treatment effects on tumour hypoxia, cMET expression and vascular pericyte coverage (Supplementary Figure 4P–S). With both anti-angiogenics, we saw an observable increase in the hypoxia marker CA9, but no differences in cMET expression. Sunitinib also resulted in a subtle dissociation between pericytes and tumour endothelium.

Anti-VEGF mono- and combination therapy applied to early-stage disease in two mutant *Kras*-driven GEMMs

The preclinical trials described above interrogated a regression setting, ie treatment of late-stage disease. We next performed a series of prevention experiments to examine whether anti-VEGF therapy could impact early-stage disease. We hypothesized that this experiment may model certain aspects of the adjuvant setting in both human PDAC, where 15–20% of patients have resectable disease [34], and in NSCLC, where stage I–IIIa tumours are surgically excised [35]; however, primary, pre-malignant and/or non-detectable lesions could still remain post-resection.

To achieve this in PDAC mice, we began treatment at ~5 weeks of age, when mice typically harbour pancreatic intra-epithelial neoplasia (PanIN) but no ultrasound-detectable solid tumours [1,31]. In contrast to late-stage treatment, anti-VEGF mono-therapy resulted in a modest, albeit insignificant, OS benefit relative to controls, comparable to that derived from gemcitabine (Figure 5A). However, the combination resulted in an additive and significant OS benefit. Next, we assessed metastatic incidence in the RLNs and LV and found no significant differences in the probability of observing micro-metastases to either organ in any examinable treatment group; rather, we observed a trend towards an increase in the time required to detect RLN metastases in the combination group (Figure 5B, C, Supplementary Figure 5A). Note that we could not calculate a probability factor for the LV in the gemcitabine cohort because we did not observe any micro-metastases in the limited number of mice available (data not shown).

To model prevention in the NSCLC GEMM, we treated mice starting at 2 wpi, when only AAH lesions were evident, for up to 14 weeks (16 wpi), which is when mice have advanced disease and were enrolled for regression studies. Anti-VEGF mono- and combination therapy with carboplatin caused a dramatic inhibition of tumour growth compared to either control or carboplatin-treated mice, with minimal if any increase in tumour burden over the 4 week imaging interval (Figure 6A, Supplementary Figure 6A). Interestingly, carboplatin alone did not impact tumour growth in either the prevention (Figure 6A) or regression

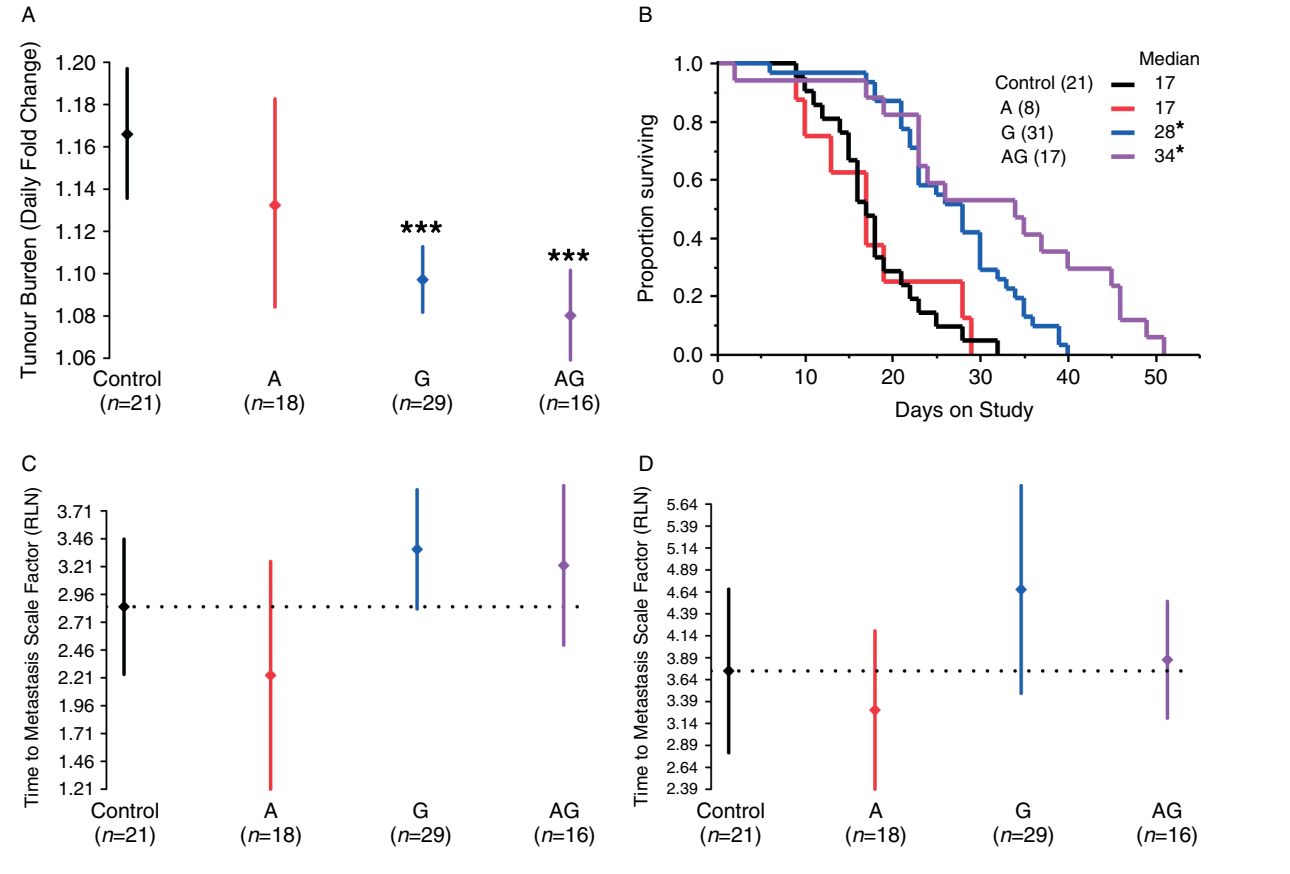

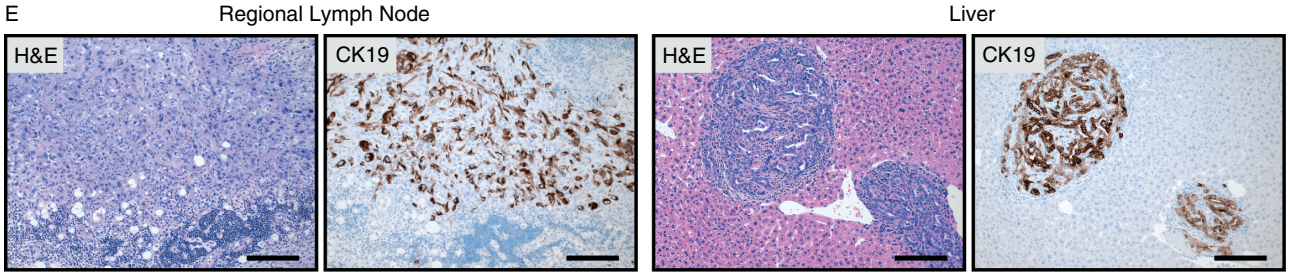

F

Treatment	PDAC, short-term (7d): # of Positive Mice / Total # Examined		
	Regional Lymph Node Metastases	Liver Metastases	Total # Mice with any Confirmed Met
Control	0/9	0/9	0/9
Anti-VEGF	1/4	0/4	1/4
Gemcitabine	1/7	1/7	2/7
Anti-VEGF+Gemcitabine	0/4	0/4	0/4

Figure 3. Anti-VEGF treatment effects on efficacy, overall survival and metastasis in a genetically engineered mouse model of PDAC, regression setting. Daily fold-change in tumour burden, as measured by high-resolution ultrasound imaging for each treatment cohort [control (black), anti-VEGF (A, red), gemcitabine (G, blue)] and the combination of anti-VEGF plus gemcitabine (AG, purple). Data are shown as mean ±95% confidence intervals; $^{***}p < 0.0005$ (A). Kaplan–Meier plots showing OS in treatment cohorts described in (A); $^{*}p < 0.05$, log-rank (B). Note: subsets of mice in (A) and (B) are reproduced with permission from [1]. Weibull scale factors estimated by modelling the probability of remaining free of metastases to the RLN (C) or LV (D) for the long-term treatment cohorts shown in (A, B). The number of mice examined per treatment cohort is indicated below each point. Data are shown as mean ±95% confidence intervals. No statistically significant differences were observed between groups. Representative H&E- and CK19 IHC-stained photomicrographs of metastatic PDAC in the RLN and LV (E). Frequency of RLN and LV micrometastases observed histologically at 7 days of treatment. No significant differences were found between any treatment groups for metastatic frequency to a given tissue (F). Mice were dosed with anti-ragweed control or anti-VEGF/B20-4.1.1 antibody i.p., 5 mg/kg, twice weekly; gemcitabine was dosed i.p., 100 mg/kg, q3d × 4. PDAC, pancreatic ductal adenocarcinoma.

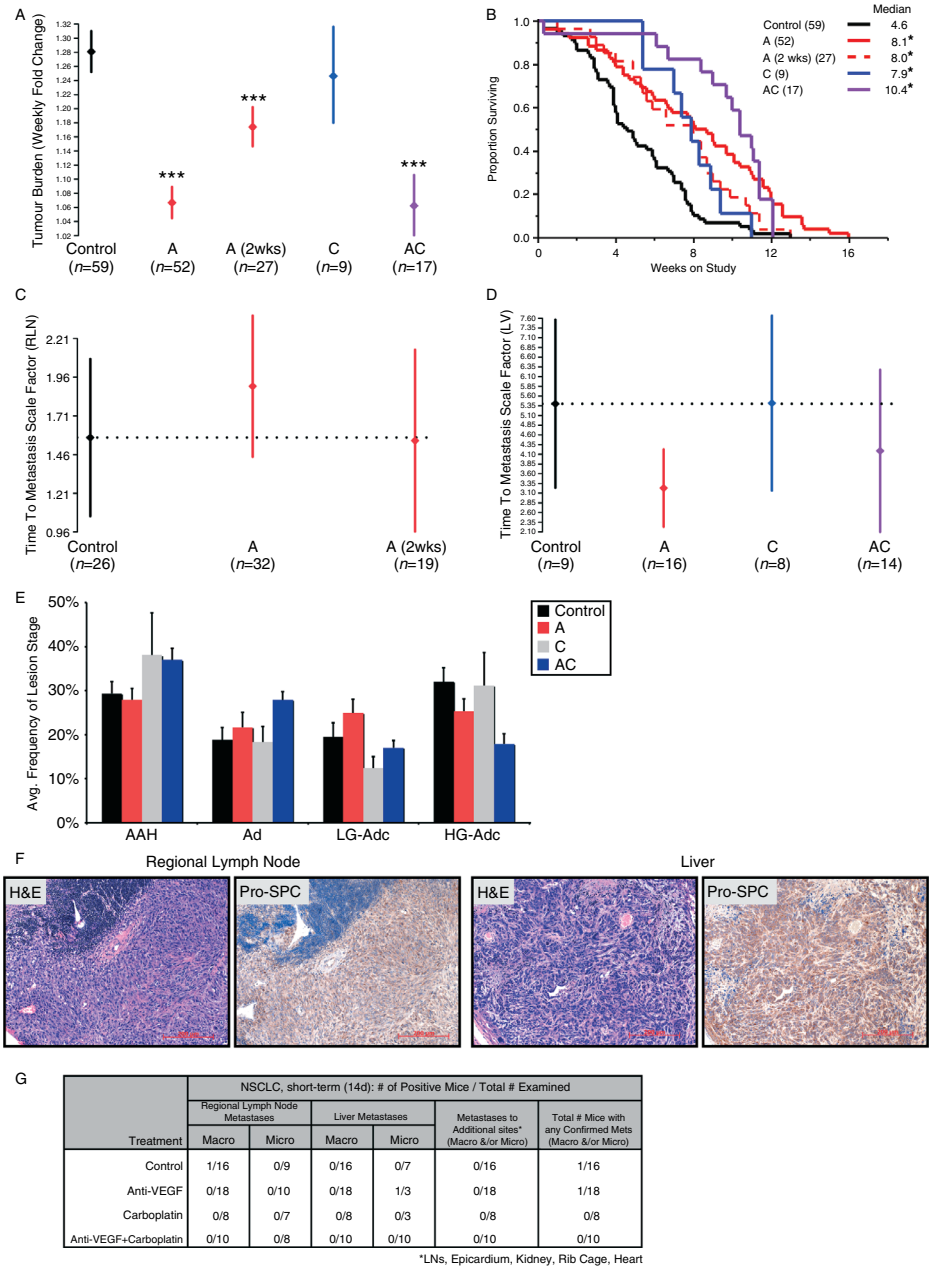

G

Treatment	NSCLC, short-term (14d): # of Positive Mice / Total # Examined					
	Regional Lymph Node Metastases		Liver Metastases		Metastases to Additional sites* (Macro &/or Micro)	Total # Mice with any Confirmed Mets (Macro &/or Micro)
	Macro	Micro	Macro	Micro		
Control	1/16	0/9	0/16	0/7	0/16	1/16
Anti-VEGF	0/18	0/10	0/18	1/3	0/18	1/18
Carboplatin	0/8	0/7	0/8	0/3	0/8	0/8
Anti-VEGF+Carboplatin	0/10	0/8	0/10	0/10	0/10	0/10

*LNs, Epicardium, Kidney, Rib Cage, Heart

Figure 4. Anti-VEGF treatment effects on primary tumour burden, overall survival and metastasis in a genetically engineered mouse model of NSCLC, regression setting. Weekly fold-change in tumour burden, as measured by micro-CT, for each treatment cohort: control (black), anti-VEGF (A, red), carboplatin (C, blue) and the combination of anti-VEGF plus carboplatin (AC, purple). Anti-VEGF monotherapy was applied using two distinct regimens: short-term/discontinuous for 2 weeks or long-term continuous therapy. Data are shown as mean $\pm$95% confidence interval; $^{***}p < 0.0005$ (A). Kaplan–Meier plots showing OS in treatment cohorts described in (A); $^{*}p < 0.05$, log-rank (B). Note: subsets of mice in (A) and (B) are reproduced with permission from [1]. Weibull scale factors estimated by modelling the probability of remaining free of metastases to the RLN (C) or LV (D) for the long-term treatment cohorts shown in (A, B). The number of mice examined per treatment cohort is indicated below each point. Data are shown as mean $\pm$95% confidence intervals. No statistically significant differences were observed between groups. Quantification of NSCLC lesion stage and grade (AAH, Ad, LG-AdC, and HG-AdC) frequency as a function of short-term (14 days) treatment with control (black bars), anti-VEGF (A, red bars), carboplatin (C, grey bars) or the combination (AC, blue bars). The frequency of each lesion stage and grade was first calculated for individual mice and then averaged across their respective treatment cohort; mean values $\pm$ SEM are depicted. The numbers of mice, total number of lesions as well as each lesion stage and grade, and average numbers of lesions per mouse analysed per treatment cohort are summarized in Supplementary Figure 4R. Statistical significance was assessed using a cumulative link mixed model fitted with the Laplace approximation. None of the observations were significantly different from one another; however, anti-VEGF + carboplatin (AC) resulted in a trend towards a decreased frequency of AdCs, with a concomitant increase in the frequency of earlier stage AAHs and Ads (E). Representative H&E- and Pro-SPC IHC-stained photomicrographs of metastatic NSCLC in the RLN and LV (F). Frequency of RLN and LV metastases observed upon gross necropsy (macro) and histological analysis (micro) in mice from the short-term treatment experiment from (E, F). No significant differences were found between any treatment groups for metastatic frequency to a given tissue or total metastatic incidence to any organ (G). Mice were dosed with anti-ragweed control or anti-VEGF/B20-4.1.1 antibody, i.p. 5 mg/kg, twice weekly; carboplatin was dosed i.p. 25 mg/kg, qd $\times$ 5 (all studies). NSCLC, non-small cell lung cancer; Micro-CT, micro-computed tomography; AAH, atypical adenomatous hyperplasia; Ad, adenoma; LG-AdC, low-grade adenocarcinoma; HG-AdC, high-grade adenocarcinoma; LNs, lymph nodes.

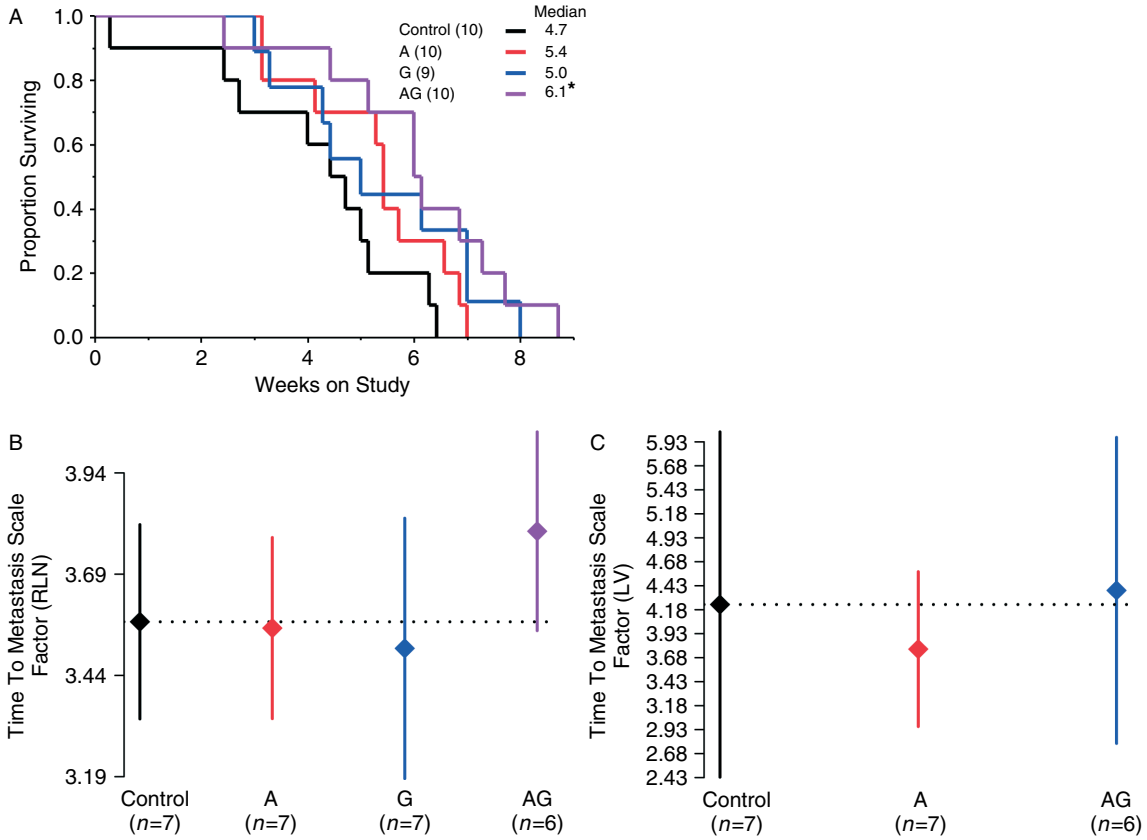

Figure 5. Anti-VEGF treatment effects on overall survival and metastasis in a genetically engineered mouse model of PDAC, prevention setting. Kaplan–Meier plots showing OS for each treatment cohort: control (black), anti-VEGF (A, red), gemcitabine (G, blue) and the combination of anti-VEGF plus gemcitabine (AG, purple); $^*p < 0.05$, log-rank (A). Weibull scale factors estimated by modelling the probability of remaining free of metastases to the RLN (B) or LV (C) for the long-term treatment cohorts shown in (A). The number of mice examined per treatment cohort is indicated below each point. Data are shown as mean ±95% confidence intervals. No statistically significant differences were observed between groups. Dosing regimens were equivalent to those listed in the legend to Figure 3.

(Figure 4A) setting. We then histologically quantitated the stages and grades of lesions present within the lungs [32,33] and found that anti-VEGF-containing regimens showed reduced numbers of lung lesions per mouse and a trend towards a decreased frequency of HG-AdC, with a concomitant increased frequency of earlier-stage AAH (Figure 6B, Supplementary Figure 6B). Finally, the animals showed rare, if any, lesions in the RLNs and LV and no significant differences between any of the groups (Figure 6C).

Discussion

Targeted therapies aimed at the VEGF signalling pathway are the only anti-angiogenic drugs currently approved for cancer treatment. Given the thousands of patients treated and the numerous clinical trials under way, it is important to understand the benefits and risks involved when using these agents [8,36]. Since VEGF can also act as a permeability factor and regulate vasodilation, it is understandable that VEGF inhibition in humans can result in risks associated with these mechanisms. However, the association with increased tumour invasion and metastasis remains controversial. Indeed, a significant number of studies over the last two decades have shown that VEGF inhibitors frequently suppress invasion and metastasis as well as primary tumour growth [12]. A known exception is glioblastoma multiforme, where it was shown that treatment with an anti-VEGF antibody increased animal survival but simultaneously resulted in more diffuse disease, owing to nests of migrating tumour cells co-opting nearby vessels [37]. Intriguingly, recent studies have emphasized some unique aspects of glioblastoma angiogenesis; glioblastoma stem-like cells were shown to differentiate into functional vascular endothelium [38,39].

The debate regarding a broader effect of VEGF pathway inhibitors on tumour invasion and metastasis has been fuelled by three recent studies, which reported that treatment with two anti-angiogenic agents targeting VEGFR-2 impeded primary tumour growth but concomitantly increased tumour invasiveness and, in some cases, metastasis [14–16]. The earlier two studies interrogated the small molecule RTKI sunitinib; one also examined the monoclonal antibody DC101, which blocks VEGFR-2 signalling, while the other carried out parallel studies with sorafenib and SU10 944. More recently, Sennino *et al* reported increases in tumour invasion and metastasis following anti-VEGF antibody treatment in a PNET model, and the abrogation of those

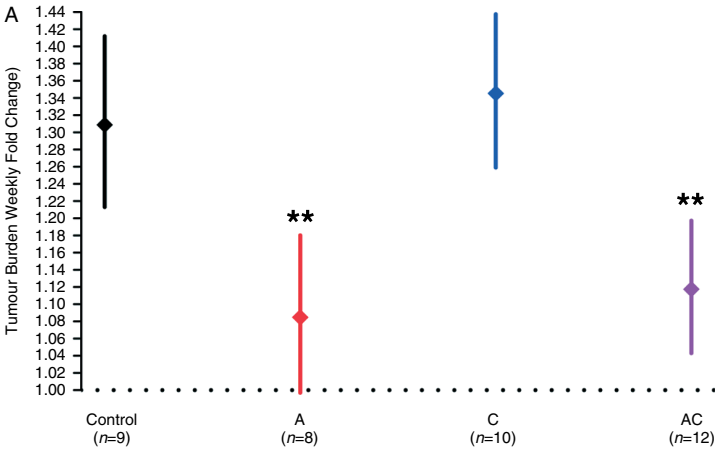

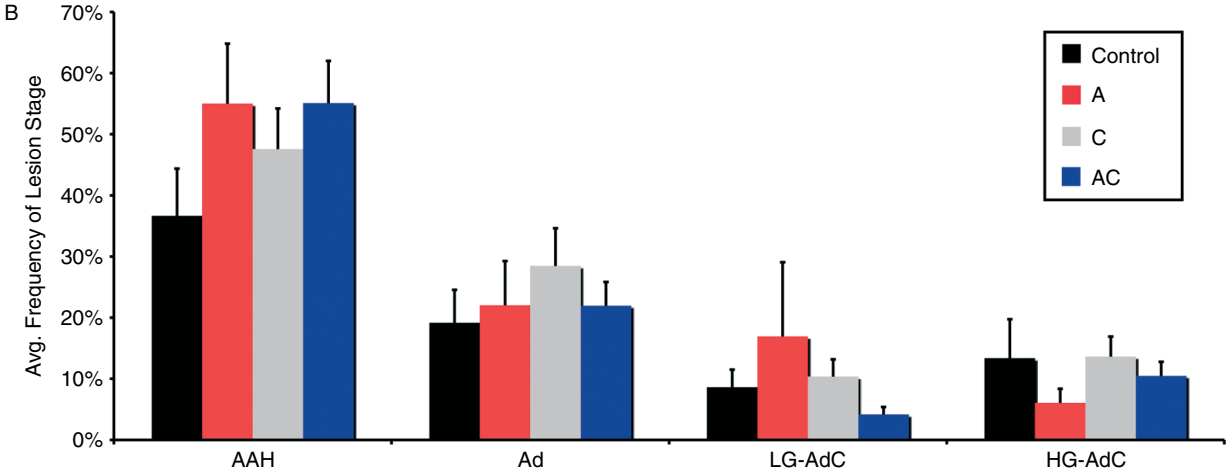

C

Treatment	NSCLC, long-term (Prevention): # of Positive Mice / Total # Examined					
	Regional Lymph Node Metastases		Liver Metastases		Metastases to Additional Sites* (Macro &/or Micro)	Total # Mice with any Confirmed Mets (Macro &/or Micro)
	Macro	Micro	Macro	Micro		
Control	1/9	0/9	0/9	0/7	2/9	2/9
Anti-VEGF	0/8	0/8	0/8	0/7	0/8	0/8
Carboplatin	0/10	0/10	0/10	0/10	1/10	1/10
Anti-VEGF+Carboplatin	0/12	0/12	0/12	0/10	1/12	1/12

*LNs, Epicardium, Kidney, Rib Cage, Heart

Figure 6. Anti-VEGF treatment effects on primary tumour growth and progression as well as metastasis in a genetically engineered mouse model of NSCLC, prevention setting. Weekly fold-change in tumour burden, as measured by micro-CT for each treatment cohort between 10 weeks (12 wpi) and ~12–14 weeks (14–16 wpi) post-study start: control (black), anti-VEGF (A, red), carboplatin (C, blue) and the combination of anti-VEGF plus carboplatin (AC, purple). Data are shown as mean ±95% confidence intervals; $^{**}p < 0.005$ (A). Quantification of NSCLC lesion stage and grade (AAH, Ad, LG-AdC and HG-AdC) frequency from the mice in (A) as a function of long-term (~12–14 weeks) treatment with control (black bars), anti-VEGF (A, red bars), carboplatin (C, grey bars) or the combination (AC, blue bars). The frequency of each lesion stage and grade was first calculated for individual mice and then averaged across their respective treatment cohort; mean values ± SEM are depicted. The numbers of mice, total number of lesions as well as each lesion stage and grade, and average numbers of lesions per mouse analysed per treatment cohort are summarized in Supplementary Figure 6B. Statistical significance was assessed using a cumulative link mixed model fitted with the Laplace approximation. None of the observations were significantly different from one another (B). Frequency of RLN and LV metastases observed upon gross necropsy (macro) and histological analysis (micro) in mice from (A, B). No significant differences were found between any treatment groups for metastatic frequency to a given tissue or total metastatic incidence to any organ (C). Dosing regimens were equivalent to those listed in the legend to Figure 4.

treatment effects upon combination treatment with anti-VEGF and small molecules targeting cMET [16]. Importantly, this study used a non-species-matched goat polyclonal antibody in the immune-competent *Rip-Tag* model, raising the concern that at least some of the observed effects are complicated by cellular immune responses directed against cross-species antibody–antigen complexes, which cannot be simulated with non-binding controls. Moreover, it remains to be determined whether endotoxin levels in the antibody

preparations/lots utilized may have contributed to their observed phenotypes. Despite extensive literature to the contrary, all three papers conveyed the idea that enhanced invasion and metastasis are general responses to all VEGF pathway inhibitors [17]. Given the broad interest in these topics among basic scientists and clinicians, we and Chung *et al* (submitted) re-examined this issue using an anti-VEGF monoclonal antibody previously validated as a murine surrogate for bevacizumab [1]. In addition to anti-VEGF monotherapy, we assessed the effects of therapeutically relevant combination regimens.

In the work described here, we analysed four different, well-validated GEMMs of cancer treated both short- and long-term with an anti-VEGF monoclonal antibody. We chose only high-bar, spontaneous tumour models, with the hypothesis that these would best inform the effects of anti-angiogenic therapy on native tumour vasculature. We performed an extensive and rigorous analysis of anti-VEGF effects in these GEMMs and found that anti-VEGF monotherapy was efficacious in two of the four models. Additionally, we found that while anti-VEGF induced a small increase in the incidence of IC2s in the *RIP-TβAg* model, it did not significantly alter the frequency of invasive disease in the two other GEMMs (SCLC or NSCLC) in which this could be assessed. Indeed, anti-VEGF mono- and combination therapy mediated a decreased trend towards more invasive lung lesions. Importantly, we did not observe a significant increase in metastatic incidence in any of the diverse, autochthonous tumour models following short- or long-term anti-VEGF mono- or combination therapy, either in advanced or early-stage disease. This is particularly notable in the PDAC GEMM, where a recent study examining two mutant *Kras* pancreatic cancer models showed that metastatic spread occurred very early during PDAC tumour progression and could be exacerbated by inflammatory agents [40]. Our data show that, in contrast, extended anti-VEGF therapy at these early stages of disease progression did not impact time to metastasis. The data from both the prevention and regression settings also indicate that, at least in the GEMMs tested, anti-VEGF dosing was tolerated for relatively long intervals, which is encouraging in light of recent clinical findings supporting the possible use of continued bevacizumab in the maintenance setting [41].

How can we explain the differences between the effects of anti-VEGF and RTKIs on tumour metastasis? To have appropriate bases for comparison between different agents, we undertook similar experiments as previously reported [15,16]. We were unable to reproduce the effects of anti-VEGF as reported by Sennino *et al*, but essentially recapitulated the previously reported effects of sunitinib on tumour burden, invasiveness and metastasis in a similar PNET model, with a corresponding increase in tumour hypoxia assessed by GLUT1 expression. Furthermore, the small increase in macro-invasive lesions resulting from anti-VEGF monoclonal therapy in our PNET model was distinct from the marked changes induced by sunitinib treatment and, more importantly, did not correlate with increased hypoxia or metastasis. It is worth noting that the baseline incidence of metastasis differs between our *RIP-TβAg* model and the *RIP-Tag* PNET model, as reported by both Paez-Ribes *et al* and Sennino *et al*. The *RIP-TβAg* model shows rare metastases at late stages, similar to previous reports documenting the incidence of metastasis in *RIP-Tag* [42,43]. Therefore, there appears to have been a drift in the *RIP-Tag* model over time and across different laboratories, evidenced by differences in observed metastases as well as median survival [15,16,44,45]. How these acquired changes may influence the response to various anti-angiogenics is currently unclear and warrants further investigation. Considering the recent approval of sunitinib for the treatment of human PNET patients [46], a retrospective analysis of metastasis patterns in sunitinib-treated PNET patients would clearly be of interest to the medical and research communities. In contrast to the PNET model, sunitinib treatment was not efficacious in the NSCLC GEMM at the same clinically relevant dose [14,15] and did not impact the neoplastic vasculature, disease invasiveness and metastatic incidence in this model. These data are interesting in light of the lack of clinical efficacy demonstrated with sorafenib in combination with chemotherapy in human NSCLC, especially given the significant overlap between the target kinase spectra of these two molecules (a similar Phase III clinical trial with sunitinib is under way) [47].

Several studies have now shown that kinase inhibitors in the same class as sunitinib target pericytes supporting the vasculature, due to their ability to inhibit PDGFR-β signalling [48], and can also up-regulate cMET expression; both of these processes may result in increased metastasis [16,49,50]. Consistent with these findings, Chung *et al* (submitted) have demonstrated that, in contrast to anti-VEGF, various RTKIs alter vessel integrity in normal endothelium and promote extravasation, seeding and survival of intravenously injected tumour cells within the lung niche. Thus, in the case of RTKIs that target VEGFR-2, published work and our findings support the hypothesis that morphological alterations in tumours do correlate with changes in the tumour vasculature and an increased incidence of metastasis. However, our results with anti-VEGF, particularly in the PNET model, caution that this is not a universal phenomenon and that changes in tumour grade can be decoupled from alterations in the incidence of metastases. Importantly, to the best of our knowledge, no clinical study has yet found convincing evidence that therapy with FDA-approved, anti-VEGF pathway agents induces a more invasive appearance in human tumours, with the possible exception of a subset of glioblastoma multiforme [37]. Indeed, several of the studies cited here, as well as our work, have demonstrated that anti-angiogenic treatment can change how tumour cells interact with the surrounding milieu. This phenomenon is not unique to this class

of drugs, as chemotherapy and other targeted therapies have both been shown to mediate metastasis in certain preclinical models/contexts [8,51]. In contrast, the recent observations that bevacizumab treatment may provide a greater benefit for advanced ovarian cancer patients at high risk for disease progression underscores the importance of context for examining the consequences of anti-angiogenic therapies [52].

The experiments and results described herein consist of a comprehensive evaluation of anti-VEGF effects on primary tumour growth, progression, invasiveness, metastasis to different sites and overall survival in a spectrum of well-validated GEMMs. These results unequivocally demonstrate that anti-VEGF monoclonal antibody therapy can be sustained without deleterious consequences in a variety of translationally relevant settings and treatment combinations. This work, along with that of Chung *et al* (submitted), also demonstrates that there are clear differences between the mechanisms by which anti-VEGF monoclonal antibody therapy and small-molecule RTKIs mediate their anti-angiogenic and anti-tumour effects. Based on the evidence presented here and in other studies, it seems rather unlikely that the acquisition of an invasive or metastatic phenotype in response to anti-VEGF treatment plays a major role in mediating resistance, which could ultimately limit therapeutic effectiveness.

Acknowledgment

We are grateful to Gunther Kauselman and Nicole Faust at Artemis for their efforts in helping design, generate and characterize the *RIP-TβAg* transgenic line. We would like to thank Greg Plowman, Dorothy French and Carlos Bais for invaluable input and critical discussions. Andres Paler-Martinez, Gloria Meng, Jianyong Wang, Jean-Michel Vernes, Aimee Fourie, Rashi Takkar, Ely Cosino, Janeko Bower, Vincent Javinal, Alfonso Arrazate, Rebecca Hong, Margaret Solon, Carmina Espiritu, Lee Nguyen, Tiffany Yuan and Alfred Wong provided excellent technical assistance. We also received extensive and invaluable technical support from the in-house pathology, genotyping and murine reproductive technology core groups. The anti-CK19 rat monoclonal antibody TROMA-III, generated by Rolf Kemler (Max-Planck Institute, Freiburg, Germany), was obtained from the Developmental Studies Hybridoma Bank, developed under the auspices of the NICHD and maintained by the the University of Iowa, Department of Biology, Iowa City, IA 52242, USA.

Author contributions

MS, SSC and LJ conceived and designed the experiments; MS, MAN, RADC and LJ supervised the experiments; MS, SSC, AL, JHC, RM, JEL, PH, AM, IK, HBR, TCC, CCKH, KHB, OF, JE-A, AJ and LJ performed and analysed the experiments; WFF, MS, AJ and LJ performed the statistical analyses; and MS, SSC, WFF, AL, NP and LJ wrote the manuscript.

Abbreviations

AAH, atypical adenomatous hyperplasia; Ad, adenoma; AdC, adenocarcinoma; CA9, carbonic anhydrase 9; CPT-11, camptothecin-11; ES-SCLC, early stage-small cell lung carcinoma; FDA, food and drug administration; GEMM, genetically engineered mouse model; GLUT1, glucose transporter 1; H&E, haematoxylin and eosin; HG-AdC, high grade-adenocarcinoma; i.p., intraperitoneal; IA, islet adenoma; IACUC, institutional animal care and use committee; IC1, micro-invasive carcinoma; IC2, macro-invasive carcinoma; IHC, immunohistochemistry; LG-AdC, low grade-adenocarcinoma; LS-SCLC; late-stage small cell lung carcinoma; LV, liver; micro-CT, micro-computed tomography; NEH, neuroendocrine hyperplasia; NSCLC, non-small cell lung carcinoma; OS, overall survival; p.o., oral; PanIN, pancreatic intra-epithelial neoplasia; PDAC, pancreatic ductal adenocarcinoma; PDGFR-β, platelet-derived growth factor receptor, β-polypeptide; Pdx1, pancreatic and duodenal homeobox 1; PFS, progression-free survival; PNET, pancreatic neuroendocrine tumour; qd, daily; RANSAC, random sample consensus; RIP, rat insulin promoter; RLN, regional lymph node; RTK, receptor tyrosine kinase; RTKI, receptor tyrosine kinase inhibitor; SCLC, small cell lung carcinoma; SV40, simian virus 40; Rb, retinoblastoma; VEGF, vascular endothelial growth factor; VEGFR-1 or -2, vascular endothelial growth factor receptor 1 or 2.

References

1. Singh M, Lima A, Molina R, *et al*. Assessing therapeutic responses in Kras mutant cancers using genetically engineered mouse models. *Nat Biotechnol* 2010; **28**: 585–593.
2. Hanahan D, Weinberg RA. The hallmarks of cancer. *Cell* 2000; **100**: 57–70.
3. Hanahan D, Weinberg RA. Hallmarks of cancer: the next generation. *Cell* 2011; **144**: 646–674.
4. Ivy SP, Wick JY, Kaufman BM. An overview of small-molecule inhibitors of VEGFR signaling. *Nat Rev Clin Oncol* 2009; **6**: 569–579.
5. Kowanetz M, Ferrara N. Vascular endothelial growth factor signaling pathways: therapeutic perspective. *Clin Cancer Res* 2006; **12**: 5018–5022.
6. Ferrara N, Hillan KJ, Gerber HP, *et al*. Discovery and development of bevacizumab, an anti-VEGF antibody for treating cancer. *Nat Rev Drug Discov* 2004; **3**: 391–400.
7. Cook KM, Figg WD. Angiogenesis inhibitors: current strategies and future prospects. *CA Cancer J Clin* 2010; **60**: 222–243.
8. Ebos JM, Kerbel RS. Antiangiogenic therapy: impact on invasion, disease progression, and metastasis. *Nat Rev Clin Oncol* 2011; **8**: 210–221.
9. Bergers G, Hanahan D. Modes of resistance to anti-angiogenic therapy. *Nat Rev Cancer* 2008; **8**: 592–603.

10. Chen HX, Cleck JN. Adverse effects of anticancer agents that target the VEGF pathway. *Nat Rev Clin Oncol* 2009; **6**: 465–477.
11. Ellis LM, Hicklin DJ. VEGF-targeted therapy: mechanisms of anti-tumour activity. *Nat Rev Cancer* 2008; **8**: 579–591.
12. Crawford Y, Ferrara N. Tumor and stromal pathways mediating refractoriness/resistance to anti-angiogenic therapies. *Trends Pharmacol Sci* 2009; **30**: 624–630.
13. Ferrara N. Pathways mediating VEGF-independent tumor angiogenesis. *Cytokine Growth Factor Rev* 2010; **21**: 21–26.
14. Ebos JM, Lee CR, Cruz-Munoz W, *et al*. Accelerated metastasis after short-term treatment with a potent inhibitor of tumor angiogenesis. *Cancer Cell* 2009; **15**: 232–239.
15. Paez-Ribes M, Allen E, Hudock J, *et al*. Antiangiogenic therapy elicits malignant progression of tumors to increased local invasion and distant metastasis. *Cancer Cell* 2009; **15**: 220–231.
16. Sennino B, Ishiguro-Oonuma T, Wei Y, *et al*. Suppression of tumor invasion and metastasis by concurrent inhibition of c-Met and VEGF signaling in pancreatic neuroendocrine tumors. *Cancer Discov* 2012; **2**: 270–287.
17. Loges S, Mazzone M, Hohensinner P, *et al*. Silencing or fueling metastasis with VEGF inhibitors: antiangiogenesis revisited. *Cancer Cell* 2009; **15**: 167–170.
18. Abate-Shen C. A new generation of mouse models of cancer for translational research. *Clin Cancer Res* 2006; **12**: 5274–5276.
19. Sharpless NE, Depinho RA. The mighty mouse: genetically engineered mouse models in cancer drug development. *Nat Rev Drug Discov* 2006; **5**: 741–754.
20. Singh M, Johnson L. Using genetically engineered mouse models of cancer to aid drug development: an industry perspective. *Clin Cancer Res* 2006; **12**: 5312–5328.
21. Hanahan D. Heritable formation of pancreatic β-cell tumours in transgenic mice expressing recombinant insulin/simian virus 40 oncogenes. *Nature* 1985; **315**: 115–122.
22. Meuwissen R, Linn SC, Linnoila RI, *et al*. Induction of small cell lung cancer by somatic inactivation of both Trp53 and Rb1 in a conditional mouse model. *Cancer Cell* 2003; **4**: 181–189.
23. Bagri A, Berry L, Gunter B, *et al*. Effects of anti-VEGF treatment duration on tumor growth, tumor regrowth, and treatment efficacy. *Clin Cancer Res* 2010; **16**: 3887–3900.
24. Bergers G, Javaherian K, Lo KM, *et al*. Effects of angiogenesis inhibitors on multistage carcinogenesis in mice. *Science* 1999; **284**: 808–812.
25. Lopez T, Hanahan D. Elevated levels of IGF-1 receptor convey invasive and metastatic capability in a mouse model of pancreatic islet tumorigenesis. *Cancer Cell* 2002; **1**: 339–353.
26. D'Angelo SP, Pietanza MC. The molecular pathogenesis of small cell lung cancer. *Cancer Biol Ther* 2010; **10**: 1–10.
27. Ganti AK, West WW, Lackner RP, *et al*. Current concepts in the diagnosis and management of small-cell lung cancer. *Oncology (Williston Park)* 2010; **24**: 1034–1039.
28. ClinicalTrials.gov at http://clinicaltrials.gov/
29. Ready NE, Dudek AZ, Pang HH, *et al*. Cisplatin, irinotecan, and bevacizumab for untreated extensive-stage small-cell lung cancer: CALGB 30306, a phase II study. *J Clin Oncol* 2011; **29**: 4436–4441.
30. Spigel DR, Greco FA, Zubkus JD, *et al*. Phase II trial of irinotecan, carboplatin, and bevacizumab in the treatment of patients with extensive-stage small-cell lung cancer. *J Thorac Oncol* 2009; **4**: 1555–1560.
31. Aguirre AJ, Bardeesy N, Sinha M, *et al*. Activated Kras and Ink4a/Arf deficiency cooperate to produce metastatic pancreatic ductal adenocarcinoma. *Genes Dev* 2003; **17**: 3112–3126.
32. Jackson EL, Olive KP, Tuveson DA, *et al*. The differential effects of mutant *p53* alleles on advanced murine lung cancer. *Cancer Res* 2005; **65**: 10280–10288.
33. Nikitin AY, Alcaraz A, Anver MR, *et al*. Classification of proliferative pulmonary lesions of the mouse: recommendations of the mouse models of human cancers consortium. *Cancer Res* 2004; **64**: 2307–2316.
34. Li D, Xie K, Wolff R, *et al*. Pancreatic cancer. *Lancet* 2004; **363**: 1049–1057.
35. Pass HI, Carbone DP, Johnson DH. *Principles and Practice of Lung Cancer: The Official Reference Text of the International Association for the Study of Lung Cancer (IASLC)*. Lippincott, Williams: & Wilkins: Philadelphia, PA: USA, 2010.
36. Reck M. Examining the safety profile of angiogenesis inhibitors: implications for clinical practice. *Target Oncol* 2010; **5**: 257–267.
37. Rubenstein JL, Kim J, Ozawa T, *et al*. Anti-VEGF antibody treatment of glioblastoma prolongs survival but results in increased vascular cooption. *Neoplasia* 2000; **2**: 306–314.
38. Ricci-Vitiani L, Pallini R, Biffoni M, *et al*. Tumour vascularization via endothelial differentiation of glioblastoma stem-like cells. *Nature* 2010; **468**: 824–828.
39. Wang R, Chadalavada K, Wilshire J, *et al*. Glioblastoma stem-like cells give rise to tumour endothelium. *Nature* 2010; **468**: 829–833.
40. Rhim AD, Mirek ET, Aiello NM, *et al*. EMT and dissemination precede pancreatic tumor formation. *Cell* 2012; **148**: 349–361.
41. Diaz-Rubio E, Gomez-Espana A, Massuti B, *et al*. First-line XELOX Plus bevacizumab followed by XELOX Plus bevacizumab or single-agent bevacizumab as maintenance therapy in patients with metastatic colorectal cancer: the Phase III MACRO TTD Study. *Oncologist* 2012; **17**: 15–25.
42. Perl AK, Dahl U, Wilgenbus P, *et al*. Reduced expression of neural cell adhesion molecule induces metastatic dissemination of pancreatic β-tumor cells. *Nat Med* 1999; **5**: 286–291.
43. Crnic I, Strittmatter K, Cavallaro U, *et al*. Loss of neural cell adhesion molecule induces tumor metastasis by up-regulating lymphangiogenesis. *Cancer Res* 2004; **64**: 8630–8638.
44. Allen E, Walters I, Hanahan D. Brivanib, an FGF/VEGF inhibitor, is differentially active 1st vs 2nd line against mouse PNET tumors developing evasive/adaptive resistance to VEGF inhibition. *Clin Cancer Res* 2011.
45. Pietras K, Hanahan D. A multitargeted, metronomic, and maximum-tolerated dose 'chemo-switch' regimen is antiangiogenic, producing objective responses and survival benefit in a mouse model of cancer. *J Clin Oncol* 2005; **23**: 939–952.
46. Raymond E, Dahan L, Raoul JL, *et al*. Sunitinib malate for the treatment of pancreatic neuroendocrine tumours. *N Engl J Med* 2011; **364**: 501–513.
47. Scagliotti G, Novello S, von Pawel J, *et al*. Phase III study of carboplatin and paclitaxel alone or with sorafenib in advanced non-small-cell lung cancer. *J Clin Oncol* 2010; **28**: 1835–1842.
48. Bergers G, Song S, Meyer-Morse N, *et al*. Benefits of targeting both pericytes and endothelial cells in the tumor vasculature with kinase inhibitors. *J Clin Invest* 2003; **111**: 1287–1295.
49. Cooke VG, Lebleu VS, Keskin D, *et al*. Pericyte depletion results in hypoxia-associated epithelial-to-mesenchymal transition and metastasis mediated by Met signaling pathway. *Cancer Cell* 2012; **21**: 66–81.
50. Xian X, Hakansson J, Stahlberg A, *et al*. Pericytes limit tumor cell metastasis. *J Clin Invest* 2006; **116**: 642–651.
51. Weis SM, Cheresh DA. Tumor angiogenesis: molecular pathways and therapeutic targets. *Nat Med* 2011; **17**: 1359–1370.
52. Perren TJ, Swart AM, Pfisterer J, *et al*. A phase 3 trial of bevacizumab in ovarian cancer. *N Engl J Med* 2011; **365**: 2484–2496.
53. *Perl AK, Wilgenbus P, Dahl U, *et al*. A causal role for E-cadherin in the transition from adenoma to carcinoma. *Nature* 1998; **392**: 190–193.

54. *Parangi S, O'Reilly M, Christofori G, *et al*. Antiangiogenic therapy of transgenic mice impairs de novo tumor growth. *Proc Natl Acad Sci USA* 1996; **93**: 2002–2007.
55. *Fuh G, Wu P, Liang WC, *et al*. Structure-function studies of two synthetic anti-vascular endothelial growth factor Fabs and comparison with the Avastin Fab. *J Biol Chem* 2006; **281**: 6625–6631.
56. *Haines BB, Bettano KA, Chenard M, *et al*. A quantitative volumetric micro-computed tomography method to analyze lung tumors in genetically engineered mouse models. *Neoplasia* 2009; **11**: 39–47.
57. *Caunt M, Mak J, Liang WC, *et al*. Blocking neuropilin-2 function inhibits tumor cell metastasis. *Cancer Cell* 2008; **13**: 331–342.
58. *Kovesi PD *MATLAB and Octave Functions for Computer Vision and Image Processing,* [cited 2011; Available from: http://www.csse.uwa.edu.au/~pk/research/matlabfns/.
59. *Brey EM, Lalani Z, Johnston C, *et al*. Automated selection of DAB-labeled tissue for immunohistochemical quantification. *J Histochem Cytochem* 2003; **51**: 575–584.
60. *Laird N and Ware JH, Random effects models for longitudinal data. *Biometrics* 1982; **38**: 963–974.
61. *Pinheiro J, Bates D, DebRoy S *et al*. nlme: Linear and Nonlinear Mixed Effects Models. R package version 3.1–97, in nlme: Linear and Nonlinear Mixed Effects Models. 2010, nlme: Linear and Nonlinear Mixed Effects Models. nlme: Linear and Nonlinear Mixed Effects Models.
62. *Gomez G, Calle ML, Oller R, *et al*. Tutorial on methods for interval-censored data and their implementation in R. *Statistical Modelling* 2009; **9**: 259–297.
63. *Zhang Z and Sun J, Interval censoring. *Stat Methods Med Res* 2010; **19**: 53–70.
64. *Collett D, *Modelling survival data in medical research 1994:* Chapman & Hall: London.
65. *Kalbfleisch JD and Prentice RL, *The Statistical Analysis of Failure Time Data* 1980; New York: John Wiley & Sons, Inc.
66. *Therneau T and Lumley T, Survival: Survival analysis, including penalised likelihood. R package version 2.36–2., in Survival: Survival analysis, including penalised likelihood. R package version 2.36–2.2010, Survival: Survival analysis, including penalised likelihood. R package version 2.36–2.
67. *RDevelopmentCoreTeam, R: A language and environment for statistical computing, in A language and environment for statistical computing, R.F.f.S. Computing, Editor 2010, R: A language and environment for statistical computing: Vienna, AustriaR: A language and environment for statistical computing.
68. *Miller RG, *Simultaneous statistical inference*. 2nd ed 1981; New York: Springer-Verlag.
69. *Bickel PJ and Doksum KA, *Mathematical Statistics* 1977; Oakland, California: Holden-Day, Inc.
70. *McCulloch CE, Searle SR, and Neuhaus JM, *Generalized, linear, and mixed models*. Second ed 2008; Wiley.
71. *Christensen RHB, ordinal: Regression Models for Ordinal Data R package version, 2012.
72. *McCullagh P and Nelder JA, *Generalized Linear Models*. Second ed 1989; Chapman & Hall.

*Cited in the online Supplementary material only.

SUPPLEMENTARY MATERIAL ON THE INTERNET

The following supplementary material may be found in the online version of this article:

Supplementary materials and methods

Supplementary Figure 1. *RIP-TβAg* PNET model: generation, validation and analysis of anti-VEGF and sunitinib effects.

Supplementary Figure 2. Characterization and preclinical trials interrogating the effects of anti-VEGF on tumour burden, invasiveness and metastasis in the $Rb^{fl/fl}$; $p53^{frt/frt}$ SCLC GEMM.

Supplementary Figure 3. Regression preclinical trials interrogating the effects of anti-VEGF on tumour burden, invasiveness and metastasis in the $Kras^{LSL-G12D}$; *p16/p19*$^{fl/fl}$; *Pdx1-Cre* PDAC GEMM.

Supplementary Figure 4. Preclinical trials in the regression setting interrogating the effects of anti-VEGF and sunitinib on tumour burden, invasiveness and metastasis in the $Kras^{LSL-G12D}$; $p53^{frt/frt}$ NSCLC GEMM.

Supplementary Figure 5. Metastases in preclinical trials in the prevention setting in the $Kras^{LSL-G12D}$; *p16/p19*$^{fl/fl}$; *Pdx1-Cre* PDAC GEMM.

Supplementary Figure 6. Preclinical trials in the prevention setting interrogating the effects of anti-VEGF on tumour burden and invasiveness in the $Kras^{LSL-G12D}$; $p53^{frt/frt}$ NSCLC GEMM.